The RNA-binding protein Orb2 is associated with microcephaly and supports centrosome asymmetry in neural stem cells

Beverly V. Robinson[1,2], Junnan Fang[1,3], Dipen S. Mehta[3,4], Joseph Buehler[5], and Dorothy A. Lerit[1]*

Author Affiliations:

1 Department of Cell Biology, Emory University School of Medicine, Atlanta, GA 30322
2 Genetics and Molecular Biology Graduate Program, Emory University, Atlanta, GA 30322
3 These authors contributed equally
4 College of Science and Mathematics, Augusta University, Augusta, GA 30912
5 Biochemistry, Cell, and Developmental Biology Graduate Program, Emory University, Atlanta, GA 30322

* Correspondence: dlerit@emory.edu

Running title: CPEB ortholog Orb2 modulates centrosome activity

Keywords: centrosome, asymmetry, neural stem cell, Orb2, CPEB, RNA-binding protein, post-transcriptional regulation, MTOC

Funding information: This work was supported by NIH grant T32GM008490 (BVR), American Heart Association postdoctoral fellowship 20POST35210023 (to JF) and NIH grant R01GM138544 (to DAL).

Abstract

To maintain a balance of self-renewal versus neurogenesis, neural stem cells (NSCs) undergo repeated cycles of asymmetric cell division along an invariant polarity axis instructed by centrosomes. During interphase, the NSC centrosomes are defined by marked asymmetries in protein composition and functional activity as microtubule-organizing centers. Here, we show a conserved RNA-binding protein, Orb2, supports centrosome asymmetry in interphase NSCs. While Orb2 localizes to the active apical centrosome, it promotes the transient inactivation of the basal centrosome required for centrosome segregation and spindle morphogenesis. Orb2 is required cell autonomously within NSCs to support centrosome asymmetry and maintenance of the stem cell pool. Conversely, loss of *orb2* manifests in microcephaly independent of Orb2 function in NSCs. We suggest Orb2 plays opposing roles in centrosome activation and inactivation, possibly through the translational regulation of multiple mRNA substrates. Bioinformatics uncovers a significant overlap among RNA targets between *Drosophila* Orb2 and human CPEB4, consistent with a conserved role for CPEB proteins in centrosome regulation and neurodevelopment.

Introduction

Neural stem cells (NSCs) undergo asymmetric cell division (ACD) along an invariant apical-basal polarity axis to segregate cell fate determinants, giving rise to two differentially fated progeny: a self-renewing stem cell and a ganglion mother cell (GMC) fated for neural differentiation (Doe et al., 1991; Knoblich et al., 1995; Kraut et al., 1996; Broadus and Doe, 1997). This balance in NSC self-renewal is critical for neurogenesis, as its deregulation can lead to brain tumors or neurodevelopmental disorders, such as microcephaly (Bond et al., 2002; Cabernard and Doe, 2009). Key to NSC homeostasis are centrosomes, which instruct the

division axis and organize the bipolar mitotic spindle required to segregate the pro-stem and pro-differentiation cell fate determinants (Cabernard and Doe, 2009; Januschke and Gonzalez, 2010; Wang et al., 2011).

Centrosomes are microtubule (MT)-organizing centers (MTOC) consisting of a central pair of centrioles surrounded by pericentriolar material (PCM), which recruits the γ-Tubulin (γTub) ring complex required for MT nucleation (Conduit et al., 2015). Normally, centrosomes recruit the robust levels of PCM necessary for microtubule-nucleating activity just before mitotic onset, a process called centrosome maturation (Gould and Borisy, 1977; Khodjakov and Rieder, 1999). Following mitotic exit, centrosomes shed PCM.

In NSCs, however, centrosomes are subject to an asymmetric centrosome maturation cycle, wherein the apical (daughter) centrosome recruits PCM and organizes MTs, while the basal-fated (mother) centrosome is transiently inactivated until mitotic onset (Rebollo et al., 2007; Rusan and Peifer, 2007; Conduit and Raff, 2010; Januschke et al., 2011). NSC centrosome asymmetry is implicated in apical-basal spindle pole alignment and centrosome segregation (Januschke and Gonzalez, 2010; Januschke et al., 2013; Lerit and Rusan, 2013; Ramdas Nair et al., 2016). A basic molecular framework required for NSC centrosome asymmetry involves asymmetric localization of Centrobin (Cnb) and Polo kinase to the daughter centrosome in a mechanism also requiring Wdr62 to promote centrosome maturation (Januschke et al., 2013; Ramdas Nair et al., 2016; Gallaud et al., 2020). Conversely, transient inactivation of the basal centrosome requires Bld10/Cep135, Pericentrin-like protein (PLP), and Polo-like kinase 4 (PLK4/SAK) (Lerit and Rusan, 2013; Singh et al., 2014; Gambarotto et al., 2019). Nevertheless, how centrosome asymmetry is regulated remains incompletely understood.

Intriguingly, *Cnb*, *Cep135*, *plp*, *polo*, and *Wdr62* mRNAs were identified as putative mRNA targets for the RNA-binding protein (RBP) Orb2 through an unbiased transcriptomics

87 study, raising the possibility that Orb2 might regulate centrosome asymmetry in NSCs (Stepien
88 et al., 2016). Orb2 is a member of the cytoplasmic polyadenylation element binding (CPEB)
89 proteins orthologous to mammalian CPEB2–4 and implicated in mRNA localization and
90 translational control (Huang et al., 2006; Keleman et al., 2007; Hafer et al., 2011). Although prior
91 work supports a role for *orb2* in NSC spindle orientation and neuronal specification, whether
92 Orb2 contributes to centrosome regulation is unknown (Hafer et al., 2011).
93 Here, we identify an NSC-autonomous role for Orb2 in establishing centrosome
94 asymmetry associated with misaligned spindles and NSC loss. We also identify an NSC-
95 independent role for Orb2 in regulating brain size, as *orb2* loss leads to microcephaly. Finally,
96 we examine potential targets of Orb2 and propose a revised model of asymmetric centrosome
97 maturation.
98
99
100 **Results and Discussion**
101
102 **Orb2 disrupts centrosome activity in interphase NSCs**
103 To determine if Orb2 contributes to centrosome asymmetry, we examined γTub distributions at
104 apical and basal centrosomes in wild-type (WT) vs. *orb2* null mutant NSCs during late
105 interphase, when centrosomes are normally asymmetric (Rebollo et al., 2007; Rusan and
106 Peifer, 2007). To directionally measure protein localization to centrosomes, we calculated an
107 asymmetry index (AI; *Methods*), wherein a value near 0 indicates symmetric distribution, while
108 values near 1 or -1 indicate asymmetric enrichment at the apical or basal centrosome,
109 respectively. Centrosomes visualized with the centriole marker Asterless (Asl; (Varmark et al.,
110 2007) displayed the expected symmetric distribution among apical and basal centrosomes in
111 both genotypes (mean AI $\pm$ S.D.= 0.0$\pm$0.2 for WT and 0.1$\pm$0.3 for *orb2*; Fig. 1A–C). In
112 comparison, γTub was significantly enriched on the apical centrosome in WT NSCs (Fig. 1A, C).

113 In contrast to WT, *orb2* NSCs showed impaired centrosome asymmetry, evident by increased
114 γTub localization to the basal centrosome and decreased AI values (Fig. 1B, C). γTub AI was
115 reduced by over 20% within *orb2* NSCs, as compared to WT (Fig 1C; p=0.05 by Kolmogorov-
116 Smirnov test). Consistently, ~30% of *orb2* NSCs (N= 12/40) had γTub AI values >2 S.D. from
117 the WT mean (Fig 1D; p< 0.0001 by chi-square test). Measuring the levels of γTub localized at
118 the apical and basal centrosomes revealed a 2.7-fold increase in γTub recruitment to the basal
119 centrosomes of symmetrized *orb2* NSCs relative to WT (Fig. 1E; p<0.0001 by Mann-Whitney
120 test). We conclude Orb2 primarily promotes centrosome asymmetry during interphase by
121 blocking the precocious activation of the basal centrosome, although diminished recruitment of
122 γTub to the apical centrosome may compound this effect.
123
124 **Orb2-dependent centrosome regulation is cell autonomous**
125 ACD is regulated through intrinsic and extrinsic cellular pathways (Siegrist and Doe, 2006; Doe,
126 2008). Prior work indicates Orb2 is broadly expressed throughout the larval central nervous
127 system (Keleman et al., 2007; Hafer et al., 2011). To elucidate if the reduction of centrosome
128 asymmetry observed in *orb2* mutants arose from a requirement for Orb2 within NSCs, we
129 depleted *orb2* specifically in NSCs using an *orb2* dsRNA transgene (*UAS-orb2*^{RNAi}) driven by the
130 NSC-specific *worniu* (*wor*)-*GAL4* (Albertson et al., 2004). Both the no *GAL4* control and the *wor-*
131 *GAL4>orb2*^{RNAi} (hereafter, *orb2*^{RNAi}) interphase NSCs showed equal distributions of Asl at apical
132 and basal centrosomes (Fig. 1F–H). While controls appeared WT with an enrichment of γTub on
133 the apical centrosome, a subset of *orb2*^{RNAi} NSCs (~30%; N=16/51) recruited γTub to the basal
134 centrosome precociously and showed reduced γTub at the apical centrosome (Fig. 1G–J).
135 These data indicate Orb2 promotes centrosome asymmetry cell autonomously within NSCs
136 through opposing activities at the apical and basal centrosomes.
137

138 **Loss of *orb2* is associated with supernumerary centrosomes**

139 The precocious activation of the basal centrosome is associated with errant centrosome
140 segregation during ACD, resulting in both centrosomes retained within the self-renewing stem
141 cell (Lerit and Rusan, 2013). To assay whether *orb2* loss similarly impairs centrosome
142 segregation, we quantified the frequency of supernumerary centrosomes in WT and *orb2* NSCs.
143 While >90% WT NSCs (N=25/30) had the expected 2 centrosomes, ~35% *orb2* mutant NSCs
144 (N=15/40) had extra centrosomes (Fig 2A–C; $p<0.05$ by chi-square test). A similar frequency of
145 supernumerary centrosomes was observed in $orb2^{RNAi}$ NSCs (~25%; N=13/51; $p<0.05$ by chi-
146 square test), demonstrating Orb2 functions within NSC to regulate centrosome number, likely
147 due to failed segregation of the basal centrosome to the GMC (Fig. 2D–F).

148

149 **Orb2 is required for mitotic spindle morphogenesis**

150 Given that Orb2 helps regulate centrosome activity and segregation, we next examined its role
151 in spindle orientation. During ACD, the NSC mitotic spindle normally orients along an invariant
152 apical-basal polarity axis entrained by the concerted action of multiple protein complexes
153 (Siegrist and Doe, 2005; Siller et al., 2006; Cabernard and Doe, 2009). Apical polarization is
154 initiated by the Par-complex, comprising Bazooka (Baz)/Par-3, Par-6, and atypical protein
155 kinase C (αPKC; (Kuchinke et al., 1998; Cai et al., 2003; Goldstein and Macara, 2007)).
156 Inhibitory phosphorylation events by αPKC restrict basal fate determinants and the adapter
157 protein Miranda (Mira) to the basal cortex (Betschinger et al., 2003; Atwood and Prehoda,
158 2009).

159 We examined polarity establishment in mitotic WT and *orb2* NSCs by monitoring the
160 localization of Baz and Mira. Localization of Baz to the apical cortex in late interphase initiates
161 NSC polarization (Wodarz and Huttner, 2003; Knoblich, 2008), while localization of Mira to the
162 basal cortex during mitosis represents a late polarization step (Shen et al., 1998; Rolls et al.,

163 2003; Atwood and Prehoda, 2009). WT and *orb2* mutant NSCs showed similar distributions of
164 Baz and Mira to the apical and basal cortices, respectively (Fig 2G–I; n.s. by chi-square test).
165 These data argue that polarization is not significantly disrupted in *orb2* larval NSCs.

166 We next used multiple coordinate analysis to define spindle orientation in WT and *orb2*
167 NSCs stained for β-Tubulin to label MTs, Baz, and Asl (see *Methods*; Fig. 2J–L). First, we
168 measured spindle orientation (θ_1),, the angle between the apical cortical polarity and spindle
169 alignment axes (Fig. 2J, M–N). In WT, most spindles aligned within 30° of the polarity axis, yet
170 ~20% of *orb2* NSC spindles were misoriented >30°, indicating *orb2* spindles are more
171 randomized than controls (Fig 2M, N; $p<0.0001$ by chi-square test).

172 To ascertain how defects in spindle orientation arise, we next quantified apical polarity
173 alignment, θ_2, the angle between the apical centrosome and polarity axes (Fig. 2J, O–P). The
174 anchoring of the apical centrosome to the apical cortex happens during early interphase and
175 influences polarization in NSCs and other stem cells (Yu et al., 2003; Januschke and Gonzalez,
176 2010; Inaba et al., 2015). Both WT and *orb2* NSCs showed alignment of the apical centrosome
177 to the apical polarity axis, consistent with our observations that apical polarity is unaffected in
178 *orb2* mutants (Fig. 2G-I, O-P).

179 Finally, we examined centrosome alignment, θ_3, the angle between the apical and basal
180 centrosome axes (Fig 2J, Q-R). About 90% of WT mitotic NSCs aligned the basal centrosome
181 ~180° away from the apical centrosome (Fig 2K, Q-R). In contrast, θ_3 is reduced in *orb2* NSCs
182 (Fig. 2L, Q). While the average reduction in θ_3 is not statistically significant, a subpopulation of
183 *orb2* NSCs (~20%; N=7/32 cells) show defective θ_3 <120° (Fig. 2L, Q). Consequently, spindle
184 morphogenesis is significantly impaired, resulting in a higher frequency (~25%; N=9/34 cells;
185 $p<0.0001$ by chi-square test) of bent spindles in *orb2* NSCs relative to WT (Fig 2R). Taken
186 together, these data argue the precocious activation of the basal centrosome in *orb2* NSCs
187 during interphase impairs centrosome migration to the basal cortex, resulting in aberrant spindle

188 alignment and morphology. Alternatively, *orb2* may have a distinct functions in interphase
189 centrosome asymmetry and mitotic spindle orientation.
190
191 **Loss of *orb2* results in microcephaly**
192 Defects in centrosome regulation contribute to neurodevelopmental disorders, including
193 microcephaly and intellectual disability (Robinson et al., 2020). Previous work illustrates *orb2* is
194 crucial for learning and memory in the adult *Drosophila* brain (Keleman et al., 2007; Mastushita-
195 Sakai et al., 2010; Kruttner et al., 2012; Kacsoh et al., 2015; Hervas et al., 2016; Sanguanini
196 and Cattaneo, 2018). Moreover, reduced brain volumes were noted from serial sectioning adult
197 *orb2* brains (Kruttner et al., 2012). Thus, to assess larval neurodevelopment in *orb2* mutants, we
198 measured the volume of single optic lobes from age-matched third instar larva (Link et al.,
199 2019). Compared to WT brains, *orb2* brains were significantly smaller (Fig 3A,B,E; $p<0.0001$ by
200 t-test). About 75% (N=10/13 cells) of *orb2* brains had volumes < 2-S.D. from WT, consistent
201 with microcephaly.
202 To determine if NSC loss contributes to *orb2*-dependent microcephaly, we counted the
203 number of Mira+ NSCs in control and *orb2* brains. While WT had ~80 NSCs, *orb2* mutants
204 showed a ~20% reduction with ~60 NSCs per lobe (Fig 3C,D,F; $p<0.001$ by t-test). These data
205 indicate Orb2 is required to maintain the NSC pool.
206 Are the centrosome and spindle defects observed in *orb2* mutants correlated with NSC
207 loss and/or microcephaly? To begin to address this question, we depleted *orb2* specifically in
208 NSCs and compared the brain volume of age matched $orb2^{RNAi}$ brains relative to no *GAL4*
209 controls and noted no difference (Fig. 3 G,H,K), indicating *orb2*-dependent microcephaly is
210 nonautonomous to NSCs – Orb2 is required in other cell types to affect brain size. In contrast,
211 NSC loss is a cell autonomous response to *orb2* depletion. Similar to *orb2* mutants, we detected
212 ~30% fewer NSC per optic lobe in $orb2^{RNAi}$ brains relative to no *GAL4* controls (Fig 3I,J,L;
213 $p<0.0001$ by t-test). We conclude the frequency of NSC loss in *orb2* mutants is similar to the

214 incidence of centrosome defects, arguing these responses are correlated. Moreover, NSC loss
215 may be uncoupled from *orb2*-dependent microcephaly, consistent with the idea that Orb2
216 supports neurodevelopment in multiple cellular lineages.

217 To elucidate mechanisms underlying NSC loss in *orb2* mutants, we first tested the
218 hypothesis that NSCs are eliminated by cell death. We quantified the coincidence of pro-
219 apoptotic cleaved Caspase 3 (CC3; (Fan and Bergmann, 2010)) in cells marked with the NSC-
220 specific Deadpan (Dpn) antibody (Bier et al., 1992). Similar rates of apoptosis were observed in
221 WT and *orb2* NSCs, indicating NSC loss occurs by other mechanisms (Fig S1 A–C; n.s. by t-
222 test). Another mechanism whereby NSCs may be depleted is via premature differentiation
223 (Cabernard and Doe, 2009; Lai and Doe, 2014; Abdel-Salam et al., 2020). Normally, the pro-
224 differentiation marker Prospero (Pros) is confined to the nucleus of the differentiating GMCs and
225 absent from NSCs (Doe et al., 1991; Vaessin et al., 1991), while retention of Pros in the NSC
226 nucleus promotes premature differentiation (Lai and Doe, 2014). We quantified the coincidence
227 of Pros with Dpn and detected no significant difference relative to WT, indicating premature
228 differentiation does not precipitate NSC loss in *orb2* mutants (Fig S1D–F; n.s. by t-test).

229 Finally, we examined whether *orb2* affects mitotic progression, reasoning impaired NSC
230 self-renewal might contribute to NSC loss. However, the mitotic indices in WT and *orb2* brains
231 were not significantly different (33.6±4.9% per lobe in N=6 WT vs. 36.3±10.1% in N=10 *orb2*
232 brains; Fig S1G–I; n.s. by t-test). These data suggest NSC loss is not due to increased
233 quiescence. Loss of NSCs observed in *orb2* mutants may be actuated by non-apoptotic cell
234 death pathways. Alternatively, the altered neuronal specification observed in *orb2* embryos may
235 impinge upon larval neurodevelopment, resulting in fewer NSCs (Hafer et al., 2011).

236

237 **Orb2 localizes to centrosomes within cycling NSCs**

238 Our data indicate Orb2 functions autonomously within NSCs to regulate centrosome
239 asymmetry. Previous work indicates CPEB proteins localize to centrosomes in *Xenopus*

240 embryos and cultured mammalian cells (Groisman et al., 2000; Pascual et al., 2020a; Pascual
241 et al., 2020b). Although Orb2 localizes to neuronal lineages, subcellular localization of Orb2 is
242 not well defined (Keleman et al., 2007; Hafer et al., 2011). Therefore, to inform mechanisms of
243 how Orb2 functions within NSCs to support centrosome asymmetry and spindle morphogenesis,
244 we examined endogenous Orb2 localization in NSCs using monoclonal antibodies (Hafer et al.,
245 2011). In interphase NSCs, Orb2 appeared dispersed throughout the cytoplasm with a notable
246 enrichment on the apical centrosome (Fig 4A, *interphase*). Apical centrosome enrichment of
247 Orb2 was observed in N=21/24 interphase NSCs, indicated by positive Orb2 AI values (Fig. 4B).
248 On average, interphase apical centrosomes contained 1.7-fold more Orb2 than basal
249 centrosomes (Fig. 4C; $p<0.01$ by t-test). Upon mitotic entry, Orb2 localization increased at both
250 centrosomes, demonstrating Orb2 is recruited to active centrosomes during centrosome
251 maturation (Fig 4A, *prophase* and *metaphase*). Our localization analysis reveals two populations
252 of Orb2 in interphase NSCs, a cytoplasmic versus centrosomal pool, raising the possibility that
253 Orb2 may normally function to regulate centrosome activity locally at centrosomes, from a
254 distance within the cytoplasm, or both.
255
256
257 **Orb2 regulates PLP protein levels in larval brains**
258 Because Orb2 is an RNA-binding protein known to promote or repress translation of its target
259 mRNAs, we reasoned it may contribute to centrosome regulation indirectly through regulation of
260 an mRNA associated with centrosome asymmetry (Mastushita-Sakai et al., 2010; Xu et al.,
261 2012; Khan et al., 2015). A genome-wide analysis for mRNA targets bound by Orb2 within
262 *Drosophila* S2 cell extracts uncovered thousands of putative targets, including mRNAs of genes
263 required for NSC centrosome asymmetry, e.g., *Cep135*, *Cnb*, *plp*, *polo*, and *Wdr62* mRNAs
264 (Januschke et al., 2013; Lerit and Rusan, 2013; Singh et al., 2014; Ramdas Nair et al., 2016;
265 Stepien et al., 2016; Gallaud et al., 2020). While these transcripts were identified as potential

266 Orb2 targets, they varied in their biologic complexity (BC), a metric of reproducibility across
267 biological replicates (Licatalosi et al., 2008).

268 Aspects of the *orb2* null phenotype in NSCs resemble *plp* loss, as both mutants display
269 precocious activation of the basal centrosome in interphase NSCs coincident with
270 supernumerary centrosome and spindle defects (Lerit and Rusan, 2013). Given these
271 similarities, we tested if Orb2 regulates PLP protein expression by comparing PLP levels in WT
272 vs. *orb2* larval brain extracts. Semi-quantitative western blotting uncovered an average 30%
273 reduction in PLP in *orb2* relative to WT, suggesting Orb2 promotes PLP translation (Fig. 5A, B).
274 To assay a requirement for Orb2 in regulating PLP in NSCs, we examined PLP localization to
275 the apical versus basal centrosomes in interphase NSCs. In WT NSCs, PLP was enriched on
276 the inactive, basal centrosome, consistent with prior work (Fig. 5C; (Lerit and Rusan, 2013;
277 Singh et al., 2014). Despite a reduction in PLP levels in whole brain extracts, robust localization
278 of PLP to centrosomes was detected in *orb2* NSCs, comparable to WT (Fig. 5C, D; n.s. by
279 Kolmogorov-Smirnov test). Further, levels of PLP localized at apical vs. basal centrosomes
280 were not significantly different from WT (Fig. 5E). Taken together, these data imply Orb2-
281 dependent regulation of PLP may occur outside of NSCs and raise the possibility that other
282 Orb2 targets contribute to NSC centrosome regulation.

283 To refine the list of targets that may be involved in NSC centrosome regulation, we
284 compared the Orb2 mRNA targets identified in *Drosophila* S2 cells (Stepien et al., 2016) to a
285 recent list of mRNA targets bound by CPEB4 in HeLa cells (Pascual et al., 2020b) and identified
286 1083 overlapping genes (Fig S2A; Table S1). Gene ontology (GO) analysis for cellular
287 components uncovered a significant enrichment of organelle terms (Fig S2B). In contrast,
288 centrosome-related ontologies were not significantly enriched among the overlapping genes
289 (Fig S2C). However, because Orb2 has multiple orthologs, CPEB2-4, other putative Orb2
290 targets absent from the CPEB4 dataset are omitted from these pairwise analyses. Therefore,
291 we examined centrosome-related ontologies of Orb2 targets with a BC $\geq$ 3. This analysis

292 identified 2150 mRNAs, among which 53 mRNAs were annotated with centrosome ontologies,
293 which may be subject to Orb2 regulation (Fig. S2D; Table S1).
294
295 **Model Summary**
296 Our data indicate Orb2 is required for robust inactivation of the basal centrosome and may also
297 enhance apical centrosome activity in interphase NSCs. Orb2 also functions in other cell types
298 for normal brain size (Fig 5F). Given its local enrichment, we propose Orb2 promotes apical
299 centrosome maturation (Fig 5F, *top box*), while cytoplasmic Orb2 inactivates the basal
300 centrosome, perhaps by repressing pro-maturation factors (Fig 5F, *bottom box*). Consistent with
301 opposing activities at the apical vs. basal centrosomes, Orb2 activates or represses the
302 translation of its targets depending on its oligomerization status ((Khan et al., 2015)). This model
303 predicts cytoplasmic Orb2 is predominantly monomeric, thereby functioning as a translational
304 repressor, while centrosome-localized Orb2 is oligomerized and functions as a translational
305 activator. Whether on-site translation occurs at the apical centrosome remains to be tested and
306 specific Orb2 targets require identification.
307 Microcephaly is quite heterogenous; however, a significant number of genes associated
308 with heritable microcephaly and intellectual disability are also associated with centrosome
309 biogenesis and regulation (Thornton and Woods, 2009; Jayaraman et al., 2018; Robinson et al.,
310 2020). Our study implicates Orb2 at the intersection of these pathways.
311
312
313

314 **Materials and Methods**

315 **Fly Stocks**

316 The following strains and transgenic lines were used: y^1w^{1118} (Bloomington *Drosophila* Stock
317 Center (BDSC) #1495) was used as the WT control unless otherwise noted. *orb2* brains were
318 isolated from the homozygous null allele, $orb2^{\Delta 36}$ (gift from P. Schedl, Princeton University (Xu
319 et al., 2012)). NSC-specific depletion of *orb2* by $orb2^{RNAi}$ ($P\{TRiP.HMJ22715\}^{attP40}$; BDSC
320 #60424) was driven by $(P\{wor.GAL4.A\}^2$; BDSC #56555). All strains were maintained on
321 Bloomington formula cornmeal-agar media (Lab-Express, Inc.; Ann Arbor, MI) at 25°C in a light
322 and temperature-controlled incubator.

323

324 **Immunofluorescence**

325 Crawling third instar larva were used for dissections. Larval brains were prepared for
326 immunofluorescence as previously described (Lerit et al., 2014). Briefly, brains were dissected
327 in Schneider's *Drosophila* Medium (ThermoFisher Scientific, #21720024), fixed in 9%
328 paraformaldehyde for 15 min, blocked in PBT buffer (Phosphate Buffered Saline (PBS)
329 supplemented with 1% BSA and 0.1% Tween-20) for one hour at room temperature prior to
330 overnight incubation in primary antibodies in PBT with nutation at 4°C. Samples were further
331 blocked with modified PBT (2% BSA, 0.1% Tween-20, and 4% normal goat serum in PBS) for 1
332 hour before incubation for two hours at room temperature with secondary antibody and DAPI.
333 Brains were oriented and mounted in Aqua-Poly/Mount (Polysciences, Inc) prior to imaging.

334 The following primary antibodies were used: guinea pig anti-Asl (1:4000, gift from G.
335 Rogers, University of Arizona), mouse anti-GTU88 (γTub; 1:250–350, Sigma T6557), rabbit anti-
336 Cnn (1:4000 gift from Tim Megraw, Florida State University), guinea pig anti-PLP (1:4000, gift
337 from Nasser Rusan, NIH), rabbit anti-phospho-Histone H3 Ser10 (pH3; 1:2000, Sigma-Millipore,
338 05-570), mouse anti-β-Tub (clone E7, 1:250; Developmental Studies Hybridoma Bank (DSHB)),

339 mouse anti-Orb2 (undiluted 1:1 mix of clones 2D11 and 4G8 (DSHB); (Xu et al., 2012)), rat anti-
340 Mira (1:500, Abcam, ab197788), rabbit anti-Baz (1:2000, gift from A. Harris, University of
341 Toronto), rat anti-Dpn (1:500, Abcam, ab195173), rabbit anti-cleaved Caspase 3 (CC3, 1:75;
342 Cell Signaling Technology, 9661s), and mouse anti-Pros (clone MR1A, 1:500; DSHB).
343 Secondary antibodies: Alexa Fluor 488, 568, and 647 (1:500, Molecular Probes). DAPI
344 (ThermoFisher Scientific) was used at 10 ng/mL.
345
346 **Microscopy**
347 Images were acquired on a Nikon Ti-E inverted microscope fitted with a Yokogawa CSU-X1
348 spinning disk head (Yokogawa Corp. of America), Orca Flash 4.0 v2 CMOS camera
349 (Hamamatsu Corp.), Perfect Focus system (Nikon), and a Nikon LU-N4 solid-state laser launch
350 (15 mW; 405, 488, 561, and 647 nm) using the following Nikon objectives: 100x 1.49-NA Apo
351 Total Internal Reflection Fluorescence oil immersion, 40x 1.3-NA Plan Fluor oil immersion, and
352 2x× 0.75-NA Plan Apo. Images were acquired at 25°C through Nikon Elements AR software on
353 a 64-bit HP Z440 workstation (Hewlett-Packard).
354
355 **Image analysis**
356 Images were assembled using Fiji (National Institutes of Health;(Schindelin et al., 2012)), Adobe
357 Photoshop, and Adobe Illustrator software to separate or merge channels, crop regions of
358 interest, generate maximum-intensity projections, and adjust brightness and contrast.
359
360 *Centrosome asymmetry*
361 Interphase NSCs were identified by the absence of pH3, round nuclear morphology, and
362 presence of duplicated centrosomes in large ($\geq$10 μm) cells. To blind the experimenter to
363 genotype, maximum projected images were generated, randomized, and used to measure
364 background-subtracted integrated densities from regions of interest (ROIs) centered at the

365 apical or basal centrosomes. Apical centrosome integrated density (*A*) and basal centrosome
366 integrated density (*B*) were used to calculate the asymmetry index, (*A*-*B*)/(*A*+*B*) ((Lerit and
367 Rusan, 2013)). The data were then unblinded and mean ± S.D. were calculated per genotype.
368
369 *Polarity, NSC number, and mitotic index*
370 Mitotic NSCs were identified by the presence of pH3 in large, Mira+ cells. To score polarity,
371 maximum projected images were anonymized to blind the experimenter to genotype, and each
372 NSC was scored for the absence or presence of Baz or Mira crescents at the apical or basal
373 cortices, respectively. All Mira+ NSCs were counted to calculate the number of NSCs per optic
374 lobe. Mitotic index is defined as the number of Mira+, pH3+ NSCs per total Mira+ NSCs.
375
376 *Spindle morphology*
377 Z-stack images of mitotic NSCs labeled with anti-β-Tub to label the mitotic spindle, Asl to mark
378 the centrioles, and Baz to label the apical polarity axis were randomized to blind the
379 experimenter to genotype. The point tool in Fiji was used to record the X,Y, and Z coordinates of
380 four ROIs per cell: 1) center of the apical centrosome, 2) center of the basal centrosome, 3)
381 center of the Baz apical crescent, and 4) center of the DAPI+ condensed chromosomes. These
382 points were used to calculate four different vectors, and vector analysis was used to calculate
383 the angles between specified vectors. The following angles (θ) were calculated: θ_1= *spindle*
384 *orientation*, the angle between the vectors defined by points 1 and 2 (division axis) relative to
385 points 3 and 4 (polarity axis); θ_2= *apical polarity alignment* is the angle between the vectors
386 defined by points 3 and 4 (apical polarity axis) relative to points 1 and 4 (apical centrosome
387 axis); and θ_3= *centrosome alignment* is the angle between the vectors defined by points 1 and 4
388 (apical centrosome axis) relative to points 2 and 4 (basal centrosome axis). Angles that fell

389 outside ± 2 S.D. from the control mean were defined as defective. For spindle alignment, NSCs
390 with spindle angles >75° were classified as orthogonal.
391
392 *Age-matched brain volume*
393 To age match larva, 20 female virgins and 10 males of the appropriate genotype were allowed
394 to seed a vial for 24 hrs. After removal of the adults, vials were incubated at 25 °C until crawling
395 third instar larva emerged. *orb2* null progeny showed a developmental delay of 24-48 hrs as
396 compared to controls; null larva took ~7-8 days to emerge. Age-matched crawling third instar
397 larva were dissected and prepared for immunofluorescence. The entire volume of the DAPI-
398 labeled brain was imaged. Imaris software (Oxford Instruments) was used to select an ROI of
399 the optic lobe and measure the volume using the 3D surfaces tool (Link et al., 2019).
400
401 *NSC differentiation and death rate*
402 NSCs were identified by the presence of Dpn. To score for premature differentiation, maximum
403 projected images of Dpn and Pros stained brains were randomized to blind the experimenter to
404 genotype, and an ROI of the central brain region was used to calculate the Pearson's
405 Correlation Coefficient on background-subtracted and automatic threshold–masked images
406 using the Coloc 2 plugin for Fiji (Schindelin et al., 2012). To score cell death, a similar analysis
407 was run on Dpn and CC3 stained brains. To assess specificity of overlapping signals for both
408 experiments, the red channel (Pros or CC3) was rotated 90° clockwise, and colocalization was
409 remeasured.
410
411 **Immunoblotting**
412 Larval brain extracts were prepared from 20 crawling third instar larva dissected in Schneider's
413 medium, removed of imaginal discs, transferred to fresh media, then rinsed once in cold PBST.
414 Samples were homogenized on ice in 30 μL of fresh PBST using a cordless motor and plastic,

415 disposable homogenizer, supplemented with 20 μL 5x SDS loading buffer, boiled for 10 min at
416 95 °C, then stored at -20 °C or resolved on a commercial 7.5% polyacrylamide gel (Bio-Rad,
417 #4568023. Proteins were transferred to a 0.2 μm nitrocellulose membrane (GE Healthcare) by
418 wet transfer in a buffer containing 25 mM Tris-HCl, pH 7.6, 192 mM glycine, 10% methanol, and
419 0.02% SDS at 4 °C. Membranes were blocked in 5% dry milk in TBST (Tris-buffered saline,
420 0.05% Tween-20), washed well with TBST, and incubated overnight at 4 °C with primary
421 antibodies. After washing with TBST, membranes were incubated for 1.5 hr in secondary
422 antibodies diluted 1:5000 in TBST. Bands were visualized with Clarity ECL substrate (Bio-Rad,
423 1705061) on a Bio-Rad ChemiDoc imaging system.
424 The following primary antibodies were used: rabbit anti-PLP (1:4000, gift from Nasser
425 Rusan, NIH), guinea pig anti-Asl (1:10,000, gift from Greg Rogers, University of Arizona), and
426 mouse anti-Orb2 (1:25 dilution each of 2D11 and 4G8; DSHB, Paul Schedl, Princeton University
427 (Hafer et al., 2011)). Secondary antibodies: goat anti-mouse HRP (1:5000, ThermoFisher
428 #31430), goat anti-rabbit HRP (1:5000, ThermoFisher #31460), and goat anti-guinea pig HRP
429 (1:5000, ThermoFisher #A18769). Densitometry was measured in Adobe Photoshop and
430 protein levels are normalized to the Asl loading control. Full-size, replicated blots are available
431 to view on FigShare: https://doi.org/10.6084/m9.figshare.17052722 . The experiment was
432 repeated with three biological replicates per genotype.
433
434 **Bioinformatics**
435 Gene names were converted to FlyBase identifiers using the Flybase.org tool 'Query by
436 symbols'(Larkin et al., 2021). Overlapping genes were identified by the 'COUNT IF' function in
437 Excel and Venn diagrams were plotted in R-Studio. GO cellular component analysis was done
438 using the Panther statistical overrepresentation test (http://www.pantherdb.org/), and Fisher's

439 exact test was used to generate an adjusted p-value, i.e., false discovery rate (FDR)(Mi et al.,
440 2021) .
441
442 **Statistical analysis**
443 Data were plotted and statistical analysis performed using Microsoft Excel, GraphPad Prism,
444 and RStudio software. Normality distributions were determined using a D'Agnostino-Pearson or
445 Shapiro-Wilk normality test. Goodness-of-Fit chi-squared analysis were performed using control
446 distributions as the expected distributions. Data were further analyzed using parametric two-
447 tailed t-test, non-parametric Mann-Whitney test or Kolmogorov-Smirnov (KS) test, or an
448 appropriate post-hoc test as noted in the figure legends. Data are plotted as mean ± S.D. and
449 are representative results from at 2 or more independent experiments.
450
451
452
453 **Supplemental materials**
454
455 **Fig. S1 NSC differentiation and survival in WT vs. *orb2* mutants.** Maximum intensity
456 projections of (A) WT and (B) *orb2* brains stained with Dpn (green; NSC nuclei) and CC3 (red;
457 pro-apototic. Insets (boxes) are enlarged to the right to highlight NSCs (dashed ovals). (C)
458 Quantification of the Pearson's correlation coefficient between Dpn and CC3 from N=10 WT and
459 15 *orb2* optic lobes pooled from two replicates. The CC3 channel was rotated clockwise (90°) to
460 test for specificity of overlapping signals. (D) Maximum intensity projections of WT and (E) *orb2*
461 brains stained with Dpn (green) and Pros (red; differentiated nuclei). (F) Quantification of the
462 Pearson's correlation coefficient between Dpn and Pros from N=16 WT and 18 *orb2* optic lobes
463 pooled from two replicates. The Pros channel was rotated clockwise (90°) to test for specificity
464 of overlapping signals. In (D) and (F), each data point is from one ROI per optic lobe. (G)

465 Projected images of WT and (H) *orb2* NSCs (dashed ovals) stained for Mira (green; NSCs) and
466 the mitotic marker pH3 (red). (I) Quantification of mitotic index from N=6 WT and 10 *orb2* brains.
467 n.s., not significant by Student's t-test. Bars: (A–E) 20 µm and 8 µm (insets); (G and H) 10 µm.
468
469 **Fig. S2 Ontological analysis of Orb2 and human CPEB4.** A) Venn diagram showing relative
470 transcript pool sizes and overlap detected from the Stepien et al. Orb2 CLIP and Pascual et al.
471 CPEB4 datasets (Stepien et al., 2016; Pascual et al., 2020b). B) Top 5 gene ontologies
472 overrepresented in the overlapping transcripts by lowest raw *p* value. C) Overrepresentation
473 tests for gene ontologies implicated in the centrosome were not significant. D)
474 Overrepresentation test of genes in the Orb2 CLIPseq with BC $\geq$3 yields significant centrosome
475 ontologies. -log *p*-values are plotted with a significance cut-off of *p*=0.05, noted by the dashed
476 line and asterisk. Genes are listed in Table S1.
477
478 **Table S1. Orb2 and CPEB4 common RNA targets.** Sheet 1 lists FlyBase IDs for all transcripts
479 detected in (Stepien et al., 2016; Pascual et al., 2020b). Sheet 2 lists overlapping genes;
480 column E is sortable to list genes with centrosome ontologies. Sheet 3 lists GO terms
481 overrepresented in the overlapping genes, column J is sortable to list genes with centrosome
482 ontologies. Sheet 4 lists Orb2 targets from (Stepien et al., 2016) with BC $\geq$ 3; column F is
483 sortable to list genes with centrosome ontologies. Sheet 5 shows an overrepresentation test for
484 centrosome ontologies from the Orb2 BC $\geq$ 3 gene list. Sheet 6 lists each gene included in the
485 indicated centrosome ontologies.
486
487
488 **Competing interest statement**
489 The authors have no competing interests to declare.
490

Acknowledgements

We thank Drs. Timothy Megraw, Nasser Rusan, Greg Rogers, and Paul Schedl for gifts of reagents. We are grateful to members of the Lerit lab and Drs. Victor Faundez and Nasser Rusan for constructive feedback on the manuscript.

This work was supported by NIH grant T32GM008490 (BVR), American Heart Association grant 20POST35210023 (to JF), and R01GM138544 (to DAL).

Author contributions

Beverly V. Robinson– data curation, formal analysis, funding acquisition, investigation, methodology, visualization, writing–original draft, and writing–review & editing.

Junnan Fang– formal analysis, funding acquisition, investigation, methodology, and writing–review & editing.

Dipen S. Mehta– investigation

Joseph D. Buehler– formal analysis, software, visualization, and writing–review & editing.

Dorothy A. Lerit– conceptualization, formal analysis, funding acquisition, investigation, methodology, project administration, supervision, visualization, writing–original draft, and writing–review & editing.

512 **References**

513 Abdel-Salam, G.M.H., I.S.M. Sayed, H.H. Afifi, S.F. Abdel-Ghafar, M.R. Abouzaid, S.I. Ismail,
514 M.S. Aglan, M.Y. Issa, H.T. El-Bassyouni, G. El-Kamah, L.K. Effat, M. Eid, M.S. Zaki,
515 S.A. Temtamy, and M.S. Abdel-Hamid. 2020. Microcephalic osteodysplastic primordial
516 dwarfism type II: Additional nine patients with implications on phenotype and genotype
517 correlation. *Am. J. Med. Genet. A*. 182:1407-1420.
518 Albertson, R., C. Chabu, A. Sheehan, and C.Q. Doe. 2004. Scribble protein domain mapping
519 reveals a multistep localization mechanism and domains necessary for establishing
520 cortical polarity. *J. Cell Sci.* 117:6061-6070.
521 Atwood, S.X., and K.E. Prehoda. 2009. aPKC phosphorylates Miranda to polarize fate
522 determinants during neuroblast asymmetric cell division. *Curr. Biol.* 19:723-729.
523 Betschinger, J., K. Mechtler, and J.A. Knoblich. 2003. The Par complex directs asymmetric cell
524 division by phosphorylating the cytoskeletal protein Lgl. *Nature*. 422:326-330.
525 Bier, E., H. Vaessin, S. Younger-Shepherd, L.Y. Jan, and Y.N. Jan. 1992. deadpan, an
526 essential pan-neural gene in Drosophila, encodes a helix-loop-helix protein similar to the
527 hairy gene product. *Genes Dev.* 6:2137-2151.
528 Bond, J., E. Roberts, G.H. Mochida, D.J. Hampshire, S. Scott, J.M. Askham, K. Springell, M.
529 Mahadevan, Y.J. Crow, A.F. Markham, C.A. Walsh, and C.G. Woods. 2002. ASPM is a
530 major determinant of cerebral cortical size. *Nat. Genet.* 32:316-320.
531 Broadus, J., and C.Q. Doe. 1997. Extrinsic cues, intrinsic cues and microfilaments regulate
532 asymmetric protein localization in Drosophila neuroblasts. *Curr. Biol.* 7:827-835.
533 Cabernard, C., and C.Q. Doe. 2009. Apical/basal spindle orientation is required for neuroblast
534 homeostasis and neuronal differentiation in Drosophila. *Dev. Cell*. 17:134-141.
535 Cai, Y., F. Yu, S. Lin, W. Chia, and X. Yang. 2003. Apical complex genes control mitotic spindle
536 geometry and relative size of daughter cells in Drosophila neuroblast and pI asymmetric
537 divisions. *Cell*. 112:51-62.
538 Conduit, P.T., and J.W. Raff. 2010. Cnn dynamics drive centrosome size asymmetry to ensure
539 daughter centriole retention in Drosophila neuroblasts. *Curr. Biol.* 20:2187-2192.
540 Conduit, P.T., A. Wainman, and J.W. Raff. 2015. Centrosome function and assembly in animal
541 cells. *Nat. Rev. Mol. Cell Biol.* 16:611-624.
542 Doe, C.Q. 2008. Neural stem cells: balancing self-renewal with differentiation. *Development*.
543 135:1575-1587.
544 Doe, C.Q., Q. Chu-LaGraff, D.M. Wright, and M.P. Scott. 1991. The prospero gene specifies cell
545 fates in the Drosophila central nervous system. *Cell*. 65:451-464.
546 Fan, Y., and A. Bergmann. 2010. The cleaved-Caspase-3 antibody is a marker of Caspase-9-
547 like DRONC activity in Drosophila. *Cell Death Differ.* 17:534-539.
548 Gallaud, E., A. Ramdas Nair, N. Horsley, A. Monnard, P. Singh, T.T. Pham, D. Salvador Garcia,
549 A. Ferrand, and C. Cabernard. 2020. Dynamic centriolar localization of Polo and
550 Centrobin in early mitosis primes centrosome asymmetry. *PLoS Biol.* 18:e3000762.
551 Gambarotto, D., C. Pennetier, J.M. Ryniawec, D.W. Buster, D. Gogendeau, A. Goupil, M. Nano,
552 A. Simon, D. Blanc, V. Racine, Y. Kimata, G.C. Rogers, and R. Basto. 2019. Plk4
553 Regulates Centriole Asymmetry and Spindle Orientation in Neural Stem Cells. *Dev. Cell*.
554 50:11-24 e10.
555 Goldstein, B., and I.G. Macara. 2007. The PAR proteins: fundamental players in animal cell
556 polarization. *Dev. Cell*. 13:609-622.
557 Gould, R.R., and G.G. Borisy. 1977. The pericentriolar material in Chinese hamster ovary cells
558 nucleates microtubule formation. *J Cell Biol*. 73:601-615.
559 Groisman, I., Y.S. Huang, R. Mendez, Q. Cao, W. Theurkauf, and J.D. Richter. 2000. CPEB,
560 maskin, and cyclin B1 mRNA at the mitotic apparatus: implications for local translational
561 control of cell division. *Cell*. 103:435-447.

562 Hafer, N., S. Xu, K.M. Bhat, and P. Schedl. 2011. The Drosophila CPEB protein Orb2 has a
563 novel expression pattern and is important for asymmetric cell division and nervous
564 system function. *Genetics*. 189:907-921.
565 Hervas, R., L. Li, A. Majumdar, C. Fernandez-Ramirez Mdel, J.R. Unruh, B.D. Slaughter, A.
566 Galera-Prat, E. Santana, M. Suzuki, Y. Nagai, M. Bruix, S. Casas-Tinto, M. Menendez,
567 D.V. Laurents, K. Si, and M. Carrion-Vazquez. 2016. Molecular Basis of Orb2
568 Amyloidogenesis and Blockade of Memory Consolidation. *PLoS Biol.* 14:e1002361.
569 Huang, Y.S., M.C. Kan, C.L. Lin, and J.D. Richter. 2006. CPEB3 and CPEB4 in neurons:
570 analysis of RNA-binding specificity and translational control of AMPA receptor GluR2
571 mRNA. *EMBO J.* 25:4865-4876.
572 Inaba, M., Z.G. Venkei, and Y.M. Yamashita. 2015. The polarity protein Baz forms a platform for
573 the centrosome orientation during asymmetric stem cell division in the Drosophila male
574 germline. *Elife*. 4.
575 Januschke, J., and C. Gonzalez. 2010. The interphase microtubule aster is a determinant of
576 asymmetric division orientation in Drosophila neuroblasts. *J Cell Biol*. 188:693-706.
577 Januschke, J., S. Llamazares, J. Reina, and C. Gonzalez. 2011. Drosophila neuroblasts retain
578 the daughter centrosome. *Nat Commun*. 2:243.
579 Januschke, J., J. Reina, S. Llamazares, T. Bertran, F. Rossi, J. Roig, and C. Gonzalez. 2013.
580 Centrobin controls mother-daughter centriole asymmetry in Drosophila neuroblasts. *Nat.*
581 *Cell Biol.* 15:241-248.
582 Jayaraman, D., B.I. Bae, and C.A. Walsh. 2018. The Genetics of Primary Microcephaly. *Annu*
583 *Rev Genomics Hum Genet*. 19:177-200.
584 Kacsoh, B.Z., J. Bozler, S. Hodge, M. Ramaswami, and G. Bosco. 2015. A novel paradigm for
585 nonassociative long-term memory in Drosophila: predator-induced changes in
586 oviposition behavior. *Genetics*. 199:1143-1157.
587 Keleman, K., S. Kruttner, M. Alenius, and B.J. Dickson. 2007. Function of the Drosophila CPEB
588 protein Orb2 in long-term courtship memory. *Nat. Neurosci.* 10:1587-1593.
589 Khan, M.R., L. Li, C. Perez-Sanchez, A. Saraf, L. Florens, B.D. Slaughter, J.R. Unruh, and K.
590 Si. 2015. Amyloidogenic Oligomerization Transforms Drosophila Orb2 from a Translation
591 Repressor to an Activator. *Cell*. 163:1468-1483.
592 Khodjakov, A., and C.L. Rieder. 1999. The sudden recruitment of gamma-tubulin to the
593 centrosome at the onset of mitosis and its dynamic exchange throughout the cell cycle,
594 do not require microtubules. *J Cell Biol*. 146:585-596.
595 Knoblich, J.A. 2008. Mechanisms of asymmetric stem cell division. *Cell*. 132:583-597.
596 Knoblich, J.A., L.Y. Jan, and Y.N. Jan. 1995. Asymmetric segregation of Numb and Prospero
597 during cell division. *Nature*. 377:624-627.
598 Kraut, R., W. Chia, L.Y. Jan, Y.N. Jan, and J.A. Knoblich. 1996. Role of inscuteable in orienting
599 asymmetric cell divisions in Drosophila. *Nature*. 383:50-55.
600 Kruttner, S., B. Stepien, J.N. Noordermeer, M.A. Mommaas, K. Mechtler, B.J. Dickson, and K.
601 Keleman. 2012. Drosophila CPEB Orb2A mediates memory independent of Its RNA-
602 binding domain. *Neuron*. 76:383-395.
603 Kuchinke, U., F. Grawe, and E. Knust. 1998. Control of spindle orientation in Drosophila by the
604 Par-3-related PDZ-domain protein Bazooka. *Curr. Biol.* 8:1357-1365.
605 Lai, S.L., and C.Q. Doe. 2014. Transient nuclear Prospero induces neural progenitor
606 quiescence. *Elife*. 3.
607 Larkin, A., S.J. Marygold, G. Antonazzo, H. Attrill, G. Dos Santos, P.V. Garapati, J.L. Goodman,
608 L.S. Gramates, G. Millburn, V.B. Strelets, C.J. Tabone, J. Thurmond, and C. FlyBase.
609 2021. FlyBase: updates to the Drosophila melanogaster knowledge base. *Nucleic Acids*
610 *Res.* 49:D899-D907.
611 Lerit, D.A., K.M. Plevock, and N.M. Rusan. 2014. Live imaging of Drosophila larval neuroblasts.
612 *J Vis Exp*.

613 Lerit, D.A., and N.M. Rusan. 2013. PLP inhibits the activity of interphase centrosomes to ensure
614 their proper segregation in stem cells. *J Cell Biol*. 202:1013-1022.
615 Licatalosi, D.D., A. Mele, J.J. Fak, J. Ule, M. Kayikci, S.W. Chi, T.A. Clark, A.C. Schweitzer, J.E.
616 Blume, X. Wang, J.C. Darnell, and R.B. Darnell. 2008. HITS-CLIP yields genome-wide
617 insights into brain alternative RNA processing. *Nature*. 456:464-469.
618 Link, N., H. Chung, A. Jolly, M. Withers, B. Tepe, B.R. Arenkiel, P.S. Shah, N.J. Krogan, H.
619 Aydin, B.B. Geckinli, T. Tos, S. Isikay, B. Tuysuz, G.H. Mochida, A.X. Thomas, R.D.
620 Clark, G.M. Mirzaa, J.R. Lupski, and H.J. Bellen. 2019. Mutations in ANKLE2, a ZIKA
621 Virus Target, Disrupt an Asymmetric Cell Division Pathway in Drosophila Neuroblasts to
622 Cause Microcephaly. *Dev. Cell*. 51:713-729 e716.
623 Mastushita-Sakai, T., E. White-Grindley, J. Samuelson, C. Seidel, and K. Si. 2010. Drosophila
624 Orb2 targets genes involved in neuronal growth, synapse formation, and protein
625 turnover. *Proc. Natl. Acad. Sci. U. S. A.* 107:11987-11992.
626 Mi, H., D. Ebert, A. Muruganujan, C. Mills, L.P. Albou, T. Mushayamaha, and P.D. Thomas.
627 2021. PANTHER version 16: a revised family classification, tree-based classification
628 tool, enhancer regions and extensive API. *Nucleic Acids Res.* 49:D394-D403.
629 Pascual, R., J. Martin, F. Salvador, O. Reina, V. Chanes, A. Millanes-Romero, C. Suner, G.
630 Fernandez-Miranda, A. Bartomeu, Y.S. Huang, R.R. Gomis, and R. Mendez. 2020a. The
631 RNA binding protein CPEB2 regulates hormone sensing in mammary gland
632 development and luminal breast cancer. *Sci Adv*. 6:eaax3868.
633 Pascual, R., C. Segura-Morales, M. Omerzu, N. Bellora, E. Belloc, C.L. Castellazzi, O. Reina, E.
634 Eyras, M.M. Maurice, A. Millanes-Romero, and R. Mendez. 2020b. mRNA spindle
635 localization and mitotic translational regulation by CPEB1 and CPEB4. *RNA*.
636 Ramdas Nair, A., P. Singh, D. Salvador Garcia, D. Rodriguez-Crespo, B. Egger, and C.
637 Cabernard. 2016. The Microcephaly-Associated Protein Wdr62/CG7337 Is Required to
638 Maintain Centrosome Asymmetry in Drosophila Neuroblasts. *Cell Rep.* 14:1100-1113.
639 Rebollo, E., P. Sampaio, J. Januschke, S. Llamazares, H. Varmark, and C. Gonzalez. 2007.
640 Functionally unequal centrosomes drive spindle orientation in asymmetrically dividing
641 Drosophila neural stem cells. *Dev. Cell*. 12:467-474.
642 Robinson, B.V., V. Faundez, and D.A. Lerit. 2020. Understanding microcephaly through the
643 study of centrosome regulation in Drosophila neural stem cells. *Biochem. Soc. Trans.*
644 48:2101-2115.
645 Rolls, M.M., R. Albertson, H.P. Shih, C.Y. Lee, and C.Q. Doe. 2003. Drosophila aPKC regulates
646 cell polarity and cell proliferation in neuroblasts and epithelia. *J Cell Biol*. 163:1089-1098.
647 Rusan, N.M., and M. Peifer. 2007. A role for a novel centrosome cycle in asymmetric cell
648 division. *J Cell Biol*. 177:13-20.
649 Sanguanini, M., and A. Cattaneo. 2018. A continuous model of physiological prion aggregation
650 suggests a role for Orb2 in gating long-term synaptic information. *R Soc Open Sci*.
651 5:180336.
652 Schindelin, J., I. Arganda-Carreras, E. Frise, V. Kaynig, M. Longair, T. Pietzsch, S. Preibisch, C.
653 Rueden, S. Saalfeld, B. Schmid, J.Y. Tinevez, D.J. White, V. Hartenstein, K. Eliceiri, P.
654 Tomancak, and A. Cardona. 2012. Fiji: an open-source platform for biological-image
655 analysis. *Nat Methods*. 9:676-682.
656 Shen, C.P., J.A. Knoblich, Y.M. Chan, M.M. Jiang, L.Y. Jan, and Y.N. Jan. 1998. Miranda as a
657 multidomain adapter linking apically localized Inscuteable and basally localized Staufen
658 and Prospero during asymmetric cell division in Drosophila. *Genes Dev.* 12:1837-1846.
659 Siegrist, S.E., and C.Q. Doe. 2005. Microtubule-induced Pins/Galphai cortical polarity in
660 Drosophila neuroblasts. *Cell*. 123:1323-1335.
661 Siegrist, S.E., and C.Q. Doe. 2006. Extrinsic cues orient the cell division axis in Drosophila
662 embryonic neuroblasts. *Development*. 133:529-536.

663 Siller, K.H., C. Cabernard, and C.Q. Doe. 2006. The NuMA-related Mud protein binds Pins and
664 regulates spindle orientation in Drosophila neuroblasts. *Nat. Cell Biol.* 8:594-600.
665 Singh, P., A. Ramdas Nair, and C. Cabernard. 2014. The centriolar protein Bld10/Cep135 is
666 required to establish centrosome asymmetry in Drosophila neuroblasts. *Curr. Biol.*
667 24:1548-1555.
668 Stepien, B.K., C. Oppitz, D. Gerlach, U. Dag, M. Novatchkova, S. Kruttner, A. Stark, and K.
669 Keleman. 2016. RNA-binding profiles of Drosophila CPEB proteins Orb and Orb2. *Proc.*
670 *Natl. Acad. Sci. U. S. A.* 113:E7030-E7038.
671 Thornton, G.K., and C.G. Woods. 2009. Primary microcephaly: do all roads lead to Rome?
672 *Trends Genet.* 25:501-510.
673 Vaessin, H., E. Grell, E. Wolff, E. Bier, L.Y. Jan, and Y.N. Jan. 1991. prospero is expressed in
674 neuronal precursors and encodes a nuclear protein that is involved in the control of
675 axonal outgrowth in Drosophila. *Cell*. 67:941-953.
676 Varmark, H., S. Llamazares, E. Rebollo, B. Lange, J. Reina, H. Schwarz, and C. Gonzalez.
677 2007. Asterless is a centriolar protein required for centrosome function and embryo
678 development in Drosophila. *Curr. Biol.* 17:1735-1745.
679 Wang, C., S. Li, J. Januschke, F. Rossi, Y. Izumi, G. Garcia-Alvarez, S.S. Gwee, S.B. Soon,
680 H.K. Sidhu, F. Yu, F. Matsuzaki, C. Gonzalez, and H. Wang. 2011. An ana2/ctp/mud
681 complex regulates spindle orientation in Drosophila neuroblasts. *Dev. Cell*. 21:520-533.
682 Wodarz, A., and W.B. Huttner. 2003. Asymmetric cell division during neurogenesis in
683 Drosophila and vertebrates. *Mech. Dev.* 120:1297-1309.
684 Xu, S., N. Hafer, B. Agunwamba, and P. Schedl. 2012. The CPEB protein Orb2 has multiple
685 functions during spermatogenesis in Drosophila melanogaster. *PLoS Genet*.
686 8:e1003079.
687 Yu, F., Y. Cai, R. Kaushik, X. Yang, and W. Chia. 2003. Distinct roles of Galphai and Gbeta13F
688 subunits of the heterotrimeric G protein complex in the mediation of Drosophila
689 neuroblast asymmetric divisions. *J Cell Biol*. 162:623-633.
690

691

692 **Abbreviations used:**
693
694 ACD, asymmetric cell division
695 AI, asymmetry index
696 Asl, Asterless
697 Baz, Bazooka/PAR-3
698 BC, biologic complexity
699 Cep135, Centrosomal protein 135kDa
700 Cnb, Centrobin
701 Cnn, Centrosomin
702 γTub, γ-Tubulin
703 GMC, ganglion mother cell
704 Mira, Miranda
705 MT, microtubule
706 MTOC, microtubule-organizing center
707 NSC, neural stem cell
708 PCM, pericentriolar material
709 PLP, Pericentrin-like protein
710 Polo, Polo kinase
711 Wdr62, WD repeat domain 62
712 *w*or, *worniu*
713 WT, wild-type
714

715

716 **Figure Legends**

717 **Figure 1. Orb2 contributes to centrosome asymmetry.** Maximum intensity projections of
718 interphase NSCs (dashed circles) stained for Asl (centrioles, magenta) and γTub (PCM, cyan).
719 Solid and dashed boxes mark apical vs. basal centrosomes; enlarged at right. (A) WT NSC with
720 γTub enriched at the apical centrosome. (B) *orb2* NSC with γTub at both centrosomes. (C) AIs
721 of Asl and γTub in N=30 NSCs from n=8 WT brains and N=40 NSCs from n=10 *orb2* brains.
722 Each dot is a measurement from one cell. (D) Frequency distribution of Asl and γTub AIs in WT
723 vs. *orb2* NSCs. Light grey (outlier) values are > 2 S.D. from the control mean. (E) Scatter plot of
724 γTub levels at apical vs. basal centrosomes in N=24 NSCs from n=8 WT brains and N=10
725 symmetrized NSCs from n=7 *orb2* brains (defined as AI >2 S.D. from WT mean). (F) no *GAL4*
726 control NSCs resemble WT. (G) $orb2^{RNAi}$ NSC with γTub at both centrosomes. (H) AIs from
727 N=39 NSCs from n=6 no GAL4 brains and N=51 NSC from n=6 $orb2^{RNAi}$ brains. (I) Frequency

728 distribution of Asl and γTub AIs in control vs. *orb2*^{RNAi} brains. (J) Scatter plot of γTub at
729 centrosomes from N=39 NSCs from n=6 control brains and N=16 NSCs from n=6
730 *worGAL4>orb2*^{RNAi} brains. Mean ± SD displayed. The experiments were repeated ≥3
731 independent replicates and significance determined by (C, H) Kolmogorov-Smirnov test, (D, I)
732 chi-square test, (E, J) Mann-Whitney test: n.s., not significant; *, $p \leq 0.05$; ** $p \leq 0.01$ ***, $p<0.001$;
733 and ****, $p<0.0001$. Bars: 5 μm, 1 μm (insets).
734
735 **Figure 2. Orb2 is required for centrosome segregation and spindle morphogenesis.**
736 Maximum intensity projections of interphase NSCs (dashed circles) from (A) WT, (B) *orb2*, (D)
737 no *GAL4* control, and (E) *orb2*^{RNAi} stained for Asl (arrows). Solid and dashed boxes mark apical
738 vs. basal centrosomes; enlarged at right. (C and F) Frequency distributions of supernumerary
739 centrosomes in interphase NSCs. (G) WT and (H) *orb2* NSCs stained for Baz (apical cortex,
740 cyan), pH3 (mitotic, cyan), Mira (basal cortex, magenta), and Asl (yellow; arrowheads). (I)
741 Frequency distribution of apical Baz and/or basal Mira crescents in mitotic NSCs. (J) Cartoon
742 depicts points used to measure within mitotic NSCs: θ_1 spindle orientation, θ_2 apical polarity
743 alignment, and θ_3 centrosome alignment (*Methods*). (K) WT and (L) *orb2* NSCs stained for MTs
744 (β-Tub, magenta), Asl (yellow), Baz (cyan), and DAPI (DNA, grey). (M) Plot and (N) frequency
745 distribution of θ_1 spindle orientation. (O) Plot and (P) frequency distribution of θ_2 apical polarity
746 alignment. (Q) Plot and (R) frequency distribution of θ_3 centrosome alignment from N=33 WT
747 and N=32 *orb2* mitotic NSCs from a single experiment across two replicates. Light grey θ are >2
748 SD from the WT mean. Mean ± SD indicated; significance determined by (C, F, I, N, P, R) Chi-
749 squared test or (M, O, Q) Two-tailed t-test. n.s., not significant; *, $p<0.05$; and ****, $p<0.0001$.
750 Bars: 5 μm; 1 μm (insets).
751

752 **Figure 3. NSC-autonomous and non-autonomous Orb2 activities support**
753 **neurodevelopment.** Projected third instar larval optic lobes (dashed lines) stained for DAPI or
754 Mira. In age-matched brains, (A) WT are larger than (B) *orb2* and (C) WT have more NSCs than
755 (D) *orb2*. (E) Volume quantified from N=15 WT and 13 *orb2* brains. (F) Quantification of NSCs in
756 N=6 WT and 10 *orb2* brains. In age-matched brains, (G) no *GAL4* controls are sized as (H)
757 $orb2^{RNAi}$ brains. Yet, (I) no *GAL4* controls have more NSCs than (J) $orb2^{RNAi}$. (K) Volume and (L)
758 NSC counts quantified from N=6 brains per genotype. Brain volumes were measured from one
759 lobe per brain and normalized to the control mean (Link et al., 2019). Mean ± SD displayed.
760 Significance determined by Student's t-test: n.s., not significant; *, $p<0.05$***; and $p<0.001$.
761 Bars: 40 µm.
762
763 **Figure 4. Orb2 localizes to active NSC centrosomes.** (A) Maximum-intensity projections of
764 WT NSCs (dashed circles) stained for Asl (magenta), Cnn (PCM; yellow), and Orb2 (cyan).
765 Solid and dashed boxes note apical vs. basal centrosomes; enlarged at right. (B) Orb2 AI and
766 (C) Orb2 levels on apical vs. basal centrosomes quantified from N=24 late interphase NSCs.
767 Mean ± SD displayed; **, $p=0.003$ by Welch's t-test. Bars: 5 µm, 1 µm (inset).
768
769 **Figure 5. Orb2 regulates PLP protein levels.** (A) Immunoblot of PLP, Asl, and Orb2 proteins
770 from WT and *orb2* third instar larval brain extracts. (B) Normalized (to Asl) relative PLP levels in
771 WT and *orb2* larval brains from 3 biological replicates. (C) Max projected WT and *orb2* NSCs
772 (dashed circles) stained for γTub (magenta) and PLP (cyan). Solid and dashed boxes note
773 apical vs. basal centrosomes; enlarged at right. (D) PLP AI calculated from N=24 WT and 32
774 *orb2* interphase NSCs. (E) PLP localization to apical and basal centrosomes in N=24 WT vs.
775 N=43 *orb2* interphase NSCs. Data representative from a single experiment across 2 replicates.
776 (F) Model depicts NSC-autonomous function of Orb2 to support interphase centrosome
777 asymmetry and NSC-independent requirement for normal brain volume. Loss of *orb2* activity

778 (grey cells) impairs basal centrosome inactivation (PCM, green). Centrosome-localized Orb2
779 (WT apical; *top box*) enhances centrosome activation, perhaps by translational activation of one
780 or more targets (black, Orb2 target BC≥3; see Table S1). Conversely, cytoplasmic Orb2
781 supports basal centrosome inactivation (*bottom box*), required for centrosome separation,
782 spindle orientation, and centrosome segregation to the daughter cells. Mean ± SD displayed; *,
783 $p<0.05$ by unpaired, one-tailed t-test; n.s., not significant. Uncropped, replicated blots are
784 available to view: https://doi.org/10.6084/m9.figshare.17052722 Bars: 5 μm; insets 1 μm.
785
786

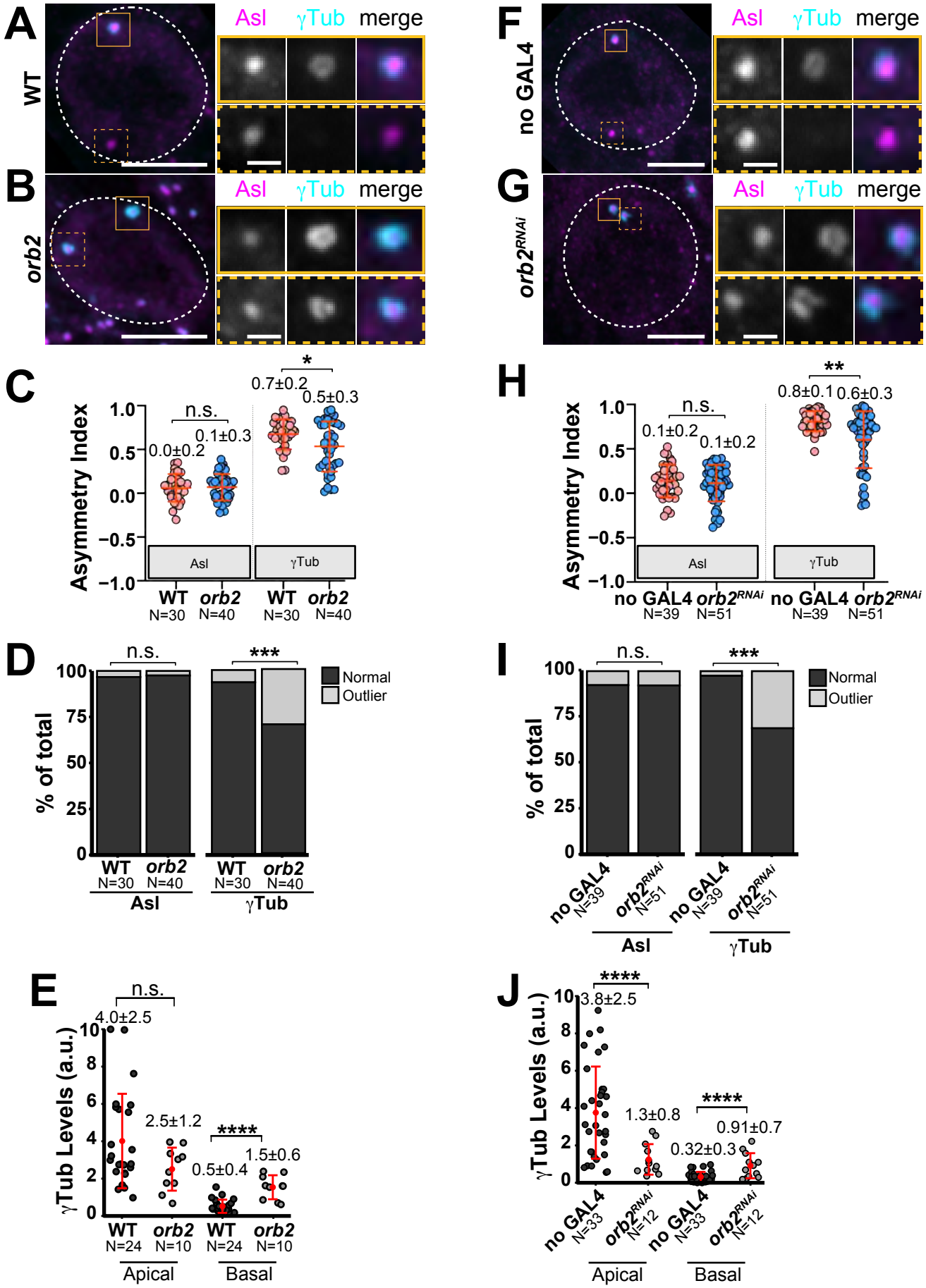

Robinson and Lerit Figure 1. orb2 is required for centrosome asymmetry

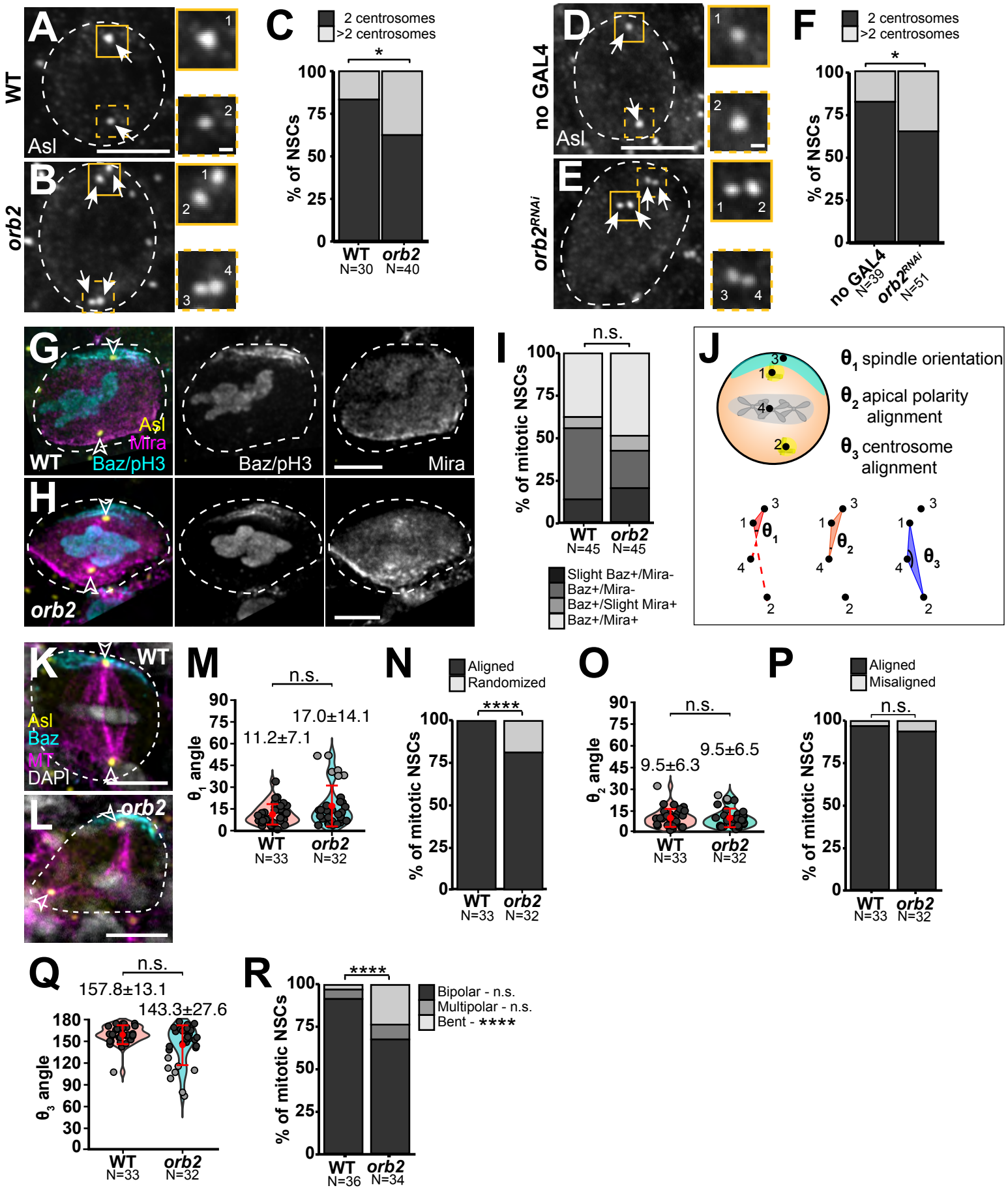

Robinson et al.
Figure 2. Orb2 is required for centrosome segregation and spindle morphogenesis

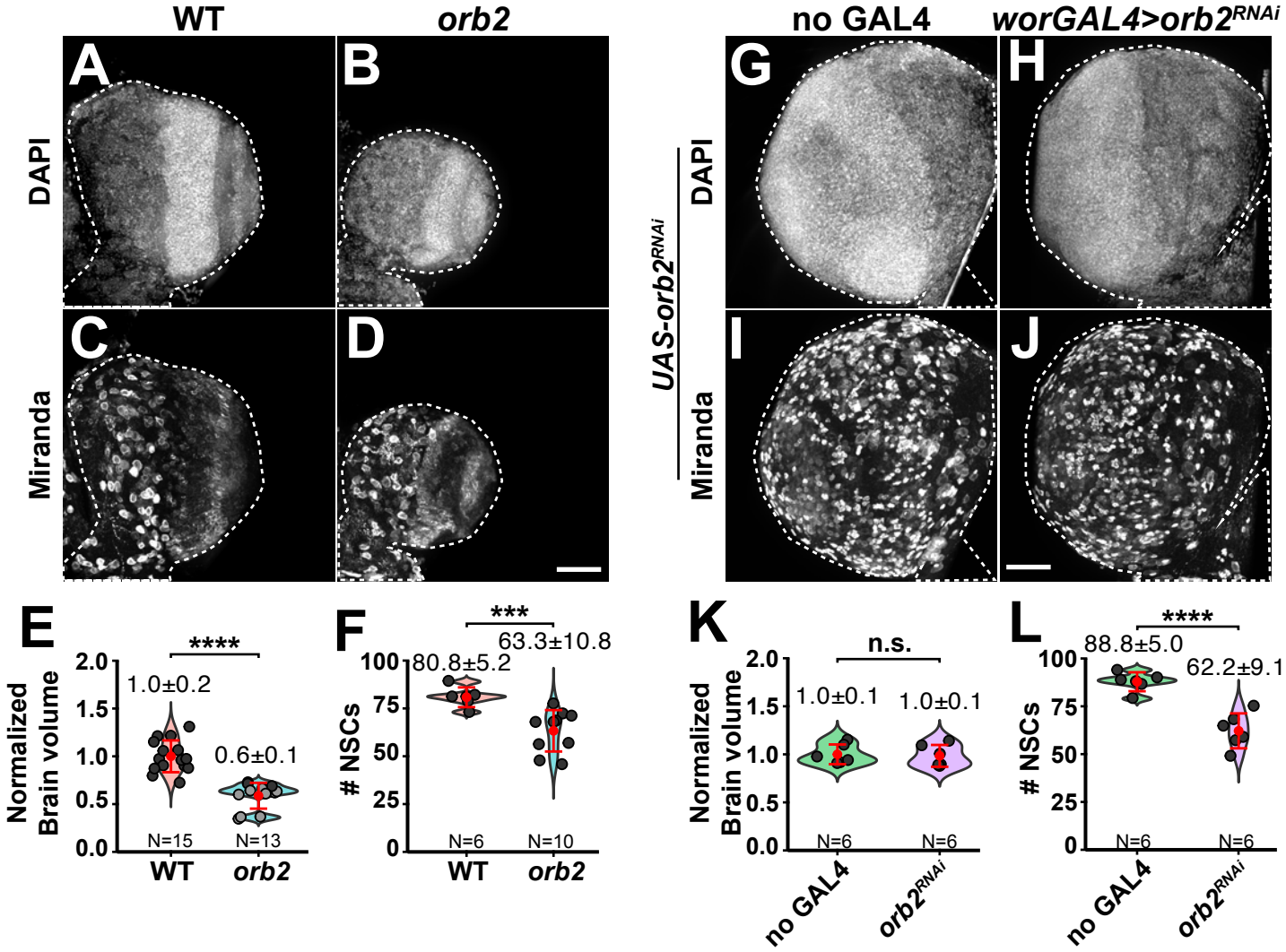

Robinson et al.
Figure 3. NSC-autonomous and non-autonomous Orb2 activities support neurodevelopment

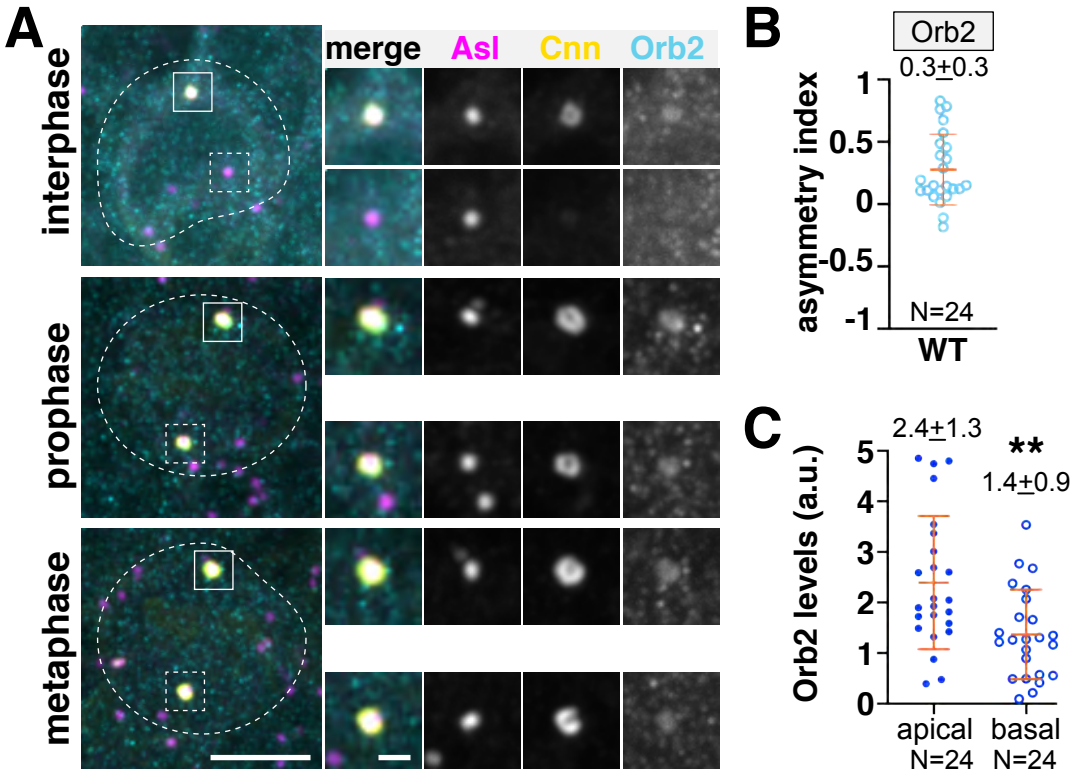

Robinson et al.
Figure 4. Orb2 localizes to active centrosomes

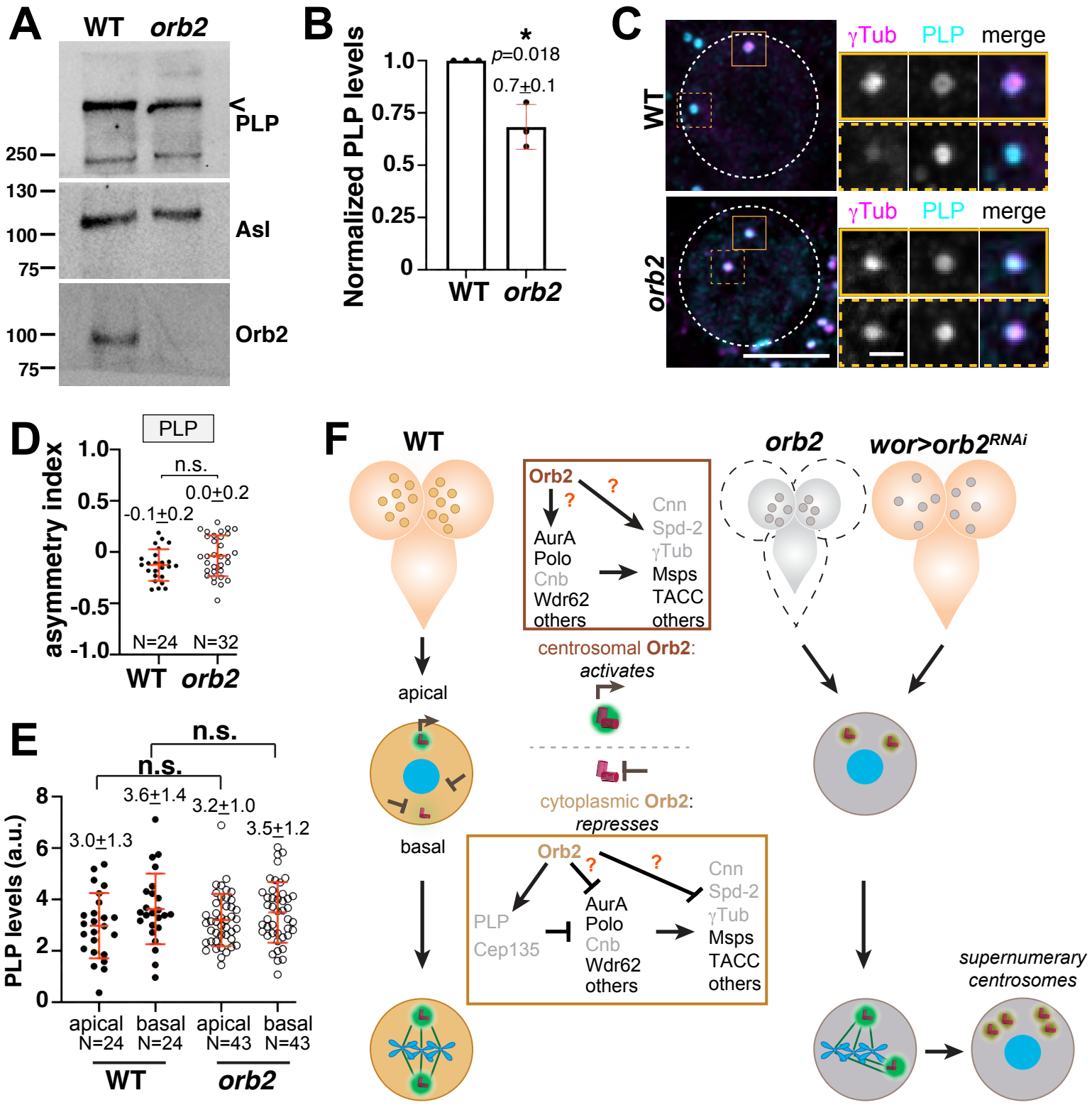

Robinson et al.
Figure 5. Orb2 regulates PLP protein levels

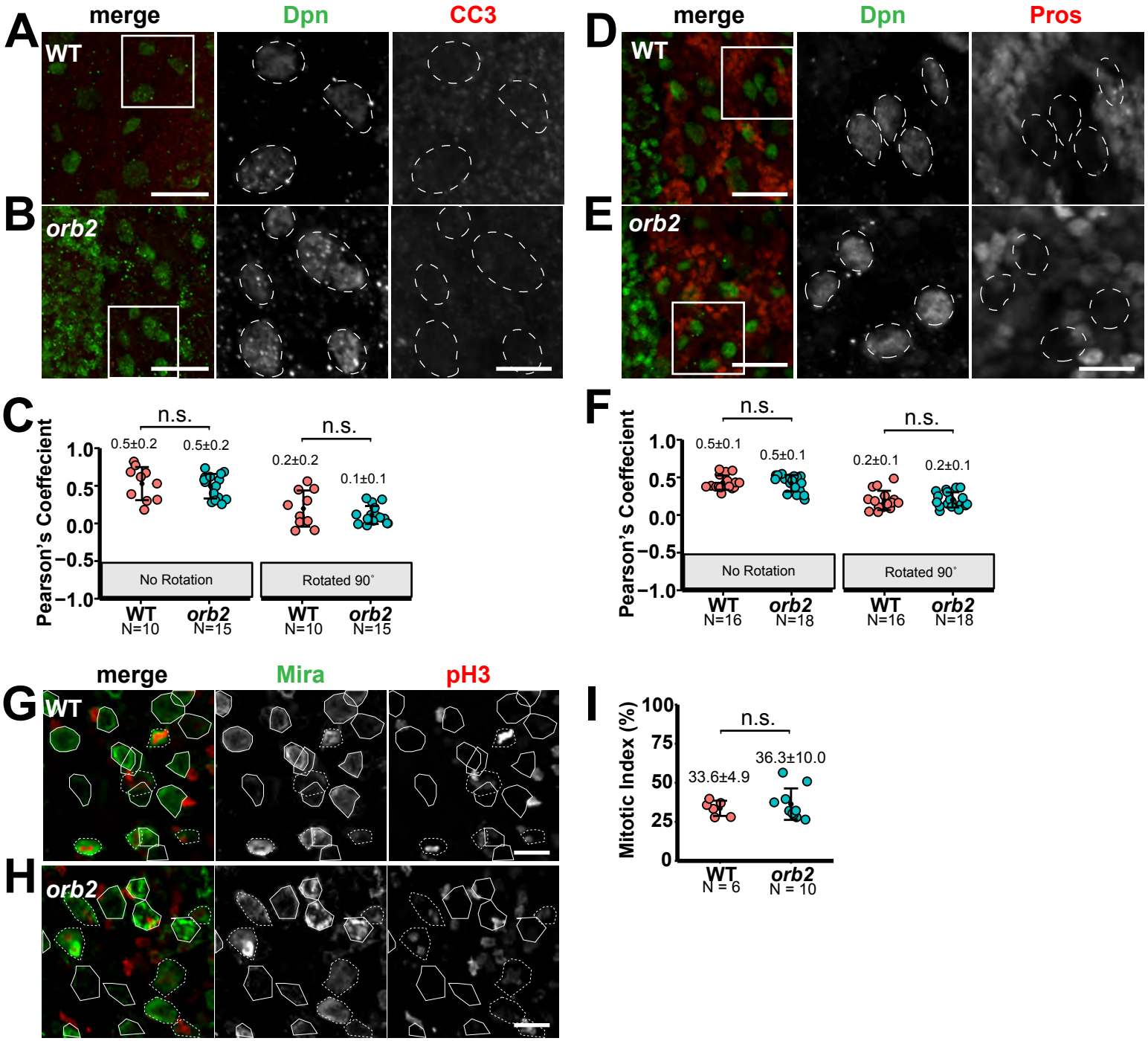

Robinson et al.
Figure S1. NSC differentiation and survival in WT vs. *orb2* mutants

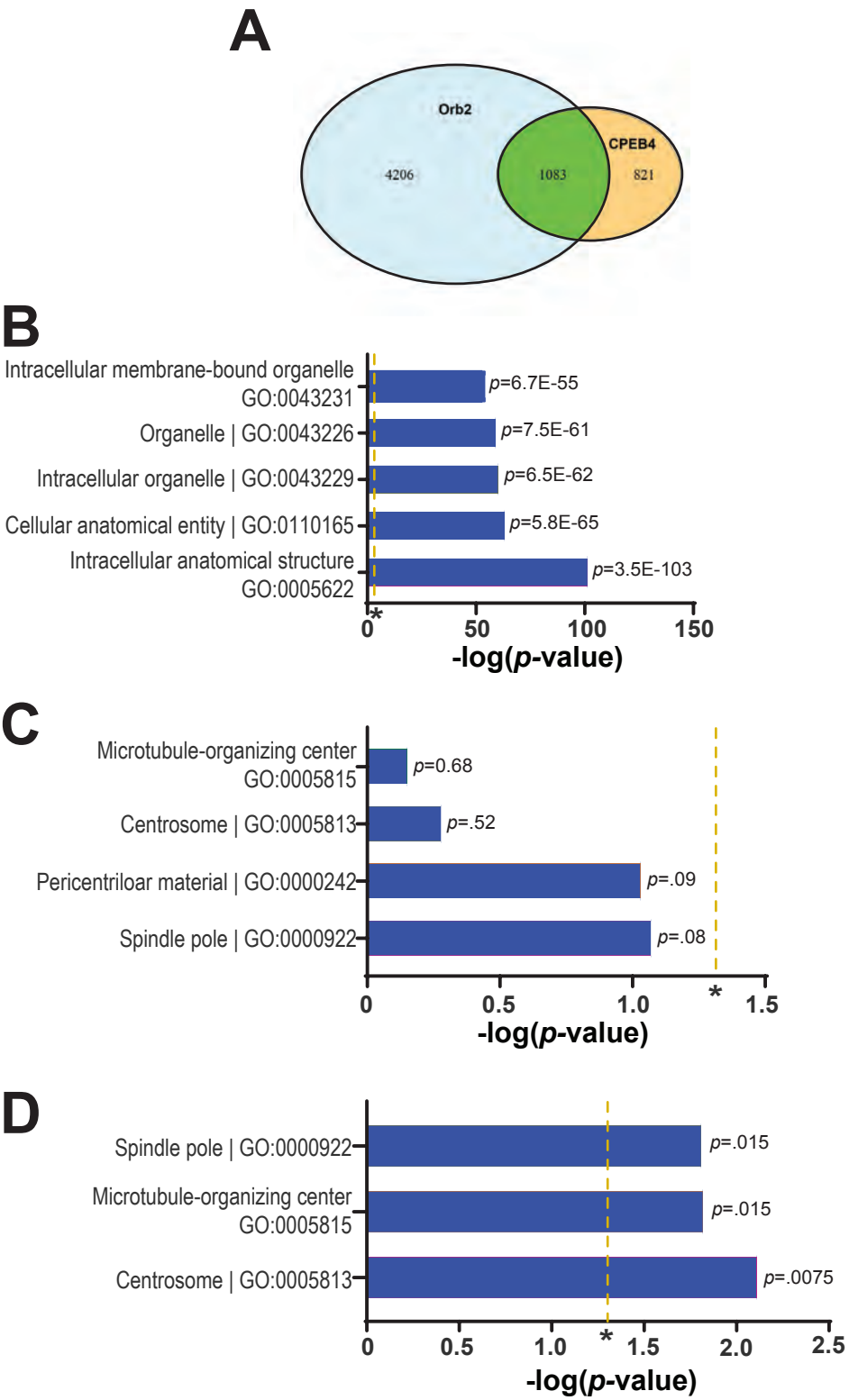

Robinson et al.
Figure S2. Ontological analysis of Orb2 and human CPEB4